

Origin of nonlocal resistance in multiterminal graphene on hexagonal-boron-nitride: Fermi surface edge states or Fermi sea topological valley currents

J. M. Marmolejo-Tejada,^{1,2} J. H. García,³ P.-H. Chang,⁴ X.-L. Sheng,^{1,5} A. Cresti,⁶ S. Roche,^{3,7} and B. K. Nikolić^{1,*}

¹*Department of Physics and Astronomy, University of Delaware, Newark, DE 19716-2570, USA*

²*School of Electrical and Electronics Engineering, Universidad del Valle, Cali, AA 25360, Colombia*

³*Catalan Institute of Nanoscience and Nanotechnology (ICN2), CSIC and The Barcelona Institute of Science and Technology, Campus UAB, Bellaterra, 08193 Barcelona, Spain*

⁴*Department of Physics and Astronomy, University of Nebraska Lincoln, Lincoln, Nebraska 68588, USA*

⁵*Department of Applied Physics, Beihang University, Beijing 100191, China*

⁶*Univ. Grenoble Alpes, CNRS, Grenoble INP, IMEP-LaHC, F-38000 Grenoble, France*

⁷*ICREA-Institució Catalana de Recerca i Estudis Avançats, 08010 Barcelona, Spain*

The recent observation [R. V. Gorbachev *et al.*, Science **346**, 448 (2014)] of nonlocal resistance R_{NL} near the Dirac point (DP) of multiterminal graphene on aligned hexagonal boron nitride (G/hBN) has been interpreted as the consequence of topological valley Hall currents carried by the Fermi sea states just beneath the bulk gap E_g induced by the inversion symmetry breaking. However, the valley Hall conductivity σ_{xy}^v , quantized inside E_g , is not directly measurable. Conversely, the Landauer-Büttiker formula, as numerically exact approach to observable nonlocal transport quantities, yields $R_{NL} \equiv 0$ for the same simplistic Hamiltonian of gapped graphene that generates $\sigma_{xy}^v \neq 0$. We combine *ab initio* with quantum transport calculations to demonstrate that G/hBN wires with zigzag edges host dispersive edge states near the DP that are absent in theories based on the simplistic Hamiltonian. Although such edge states exist also in isolated zigzag graphene wires, hBN modifies their energy-momentum dispersion to generate nonzero R_{NL} with sharp peak near the DP persisting in the presence of edge disorder. Concurrently, the edge states resolve the long-standing puzzle of why the highly insulating state of G/hBN is rarely observed. *We conclude that the observed R_{NL} is unrelated to Fermi sea topological valley currents conjectured for gapped Dirac spectra.*

The recent measurements [1] of a sharply peaked nonlocal resistance R_{NL} in a narrow energy range near the Dirac point (DP) of multiterminal graphene on hexagonal boron nitride (G/hBN) heterostructures have been interpreted as the manifestation of the valley Hall effect (VHE) [2–5]. In this interpretation, injecting charge current I_3 between leads 3 and 4 of the device illustrated in Fig. 1 generates a VH current in the first crossbar flowing from lead 1 to lead 2, which traverses the channel of length L ($\simeq 4 \mu\text{m}$ in the experiments [1]), and it is finally converted into a nonlocal voltage V_{NL} between leads 5 and 6 by the inverse VHE in the second crossbar. The corresponding nonlocal resistance $R_{NL} = V_{NL}/I_3$ has been observed previously also near the DP in multiterminal graphene due to an external magnetic field inducing edge states in the quantum Hall regime or the Zeeman spin Hall effect at higher temperatures [6–10], as well as due to the spin Hall effect [10–12] driven by adatom-induced spin-orbit coupling. However, none of these mechanisms is operational in the experiment of Ref. [1].

Instead, the physics of graphene on hBN with their crystallographic axes aligned is expected to be governed by the broken spatial inversion symmetry due to different potentials on two triangular sublattices of carbon atoms induced by the hBN substrate. This opens a gap E_g at the DP of two valleys K and K' in the band structure of an infinite two-dimensional sheet of graphene, where *ab initio* calculations have estimated

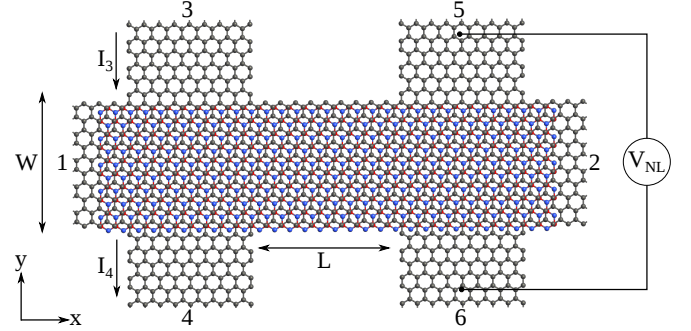


FIG. 1. (Color online) Schematic view of a six-terminal graphene, whose central region is placed onto the hBN substrate, employed in the LB-formula-based calculations of nonlocal voltage $V_{NL} = V_5 - V_6$ between leads 5 and 6 and the corresponding nonlocal resistance $R_{NL} = V_{NL}/I_3$ in response to a charge current I_3 injected between leads 3 and 4. Black, blue and red circles represent C, N and B atoms, respectively.

$E_g \simeq 58 \text{ meV}$ [14]. In addition, the finite Berry curvature [13] of opposite sign at the two valleys was predicted to generate valley-dependent transverse conductivities, $\sigma_{xy}^K = e^2/h$ and $\sigma_{xy}^{K'} = -e^2/h$ [2–4]. The VH current is characterized by the transverse VH conductivity, $\sigma_{xy}^v = \sigma_{xy}^K - \sigma_{xy}^{K'} = 2e^2/h$, and zero transverse charge conductivity, $\sigma_{xy} = \sigma_{xy}^K + \sigma_{xy}^{K'} \equiv 0$, within the gap [3, 4, 15]. Such charge-neutral valley currents, denoted also as “topological” [1–4] due to the involvement

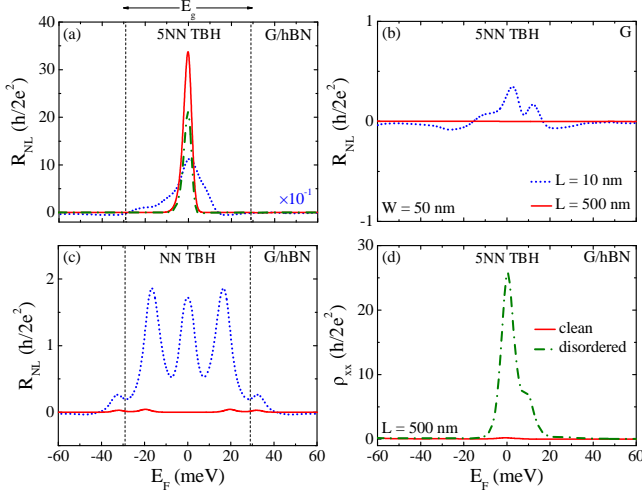


FIG. 2. (Color online). (a)–(c) Nonlocal resistance R_{NL} for the device in Fig. 1 whose channel has width $W = 50$ nm and length $L = 10$ nm or $L = 500$ nm. We use *ab initio* 5NN TBH describing G/hBN channel in (a) or isolated graphene in (b), both with zigzag edges. In panel (c), we describe G/hBN channel with zigzag edges using NN TBH [Eq. (3)] employed in prior theoretical studies [1–4, 15, 18, 29]. Panel (d) shows resistivity ρ_{xx} of edge-disordered channel of length $L = 500$ nm. The same type of disorder reduces R_{NL} peak in (a), where averaging of dash-dot line in panels (a) and (d) is performed over 10 disorder realizations. The temperature is set at $T = 20$ K, as in the experiment of Ref. [1].

of the Berry curvature hot spots in k -space, are not conserved but are expected to be long-ranged when the intervalley scattering is weak [15].

However, σ_{xy}^v is *not directly observable*, and semiclassical transport theories [16] attempting to connect σ_{xy}^v to observable nonlocal resistance [1, 4, 5]

$$R_{NL} \propto (\sigma_{xy}^v)^2 \rho_{xx}^3, \quad (1)$$

are not applicable [17] to electronic transport near the DP. In the case of G/hBN, this is further emphasized [18] by the presence of the gap forcing electrons to tunnel through the system, which is a phenomenon with no classical analog. The Landauer-Büttiker (LB) formalism [19–21]—which offers a rigorous quantum transport framework to compute V_{NL} and R_{NL} , and has been used for decades to model nonlocal transport measurements [22, 23]—yields $R_{NL} \equiv 0$ near the DP in Fig. 2(c) in multiterminal geometries whose channel length is larger than its width ($L/W \simeq 4$ in the experiments of Ref. [1]). The numerically exact result in Fig. 2(c), for a G/hBN system described by the same simplistic Hamiltonian employed [1–4, 15] to obtain $\sigma_{xy}^v \neq 0$, is also clearly incompatible with the interpretation of $R_{NL} \neq 0$ based on the picture of topological valley currents carried by the Fermi sea states just beneath the gap [3]. Such currents are conjectured to be persistent and circulating in

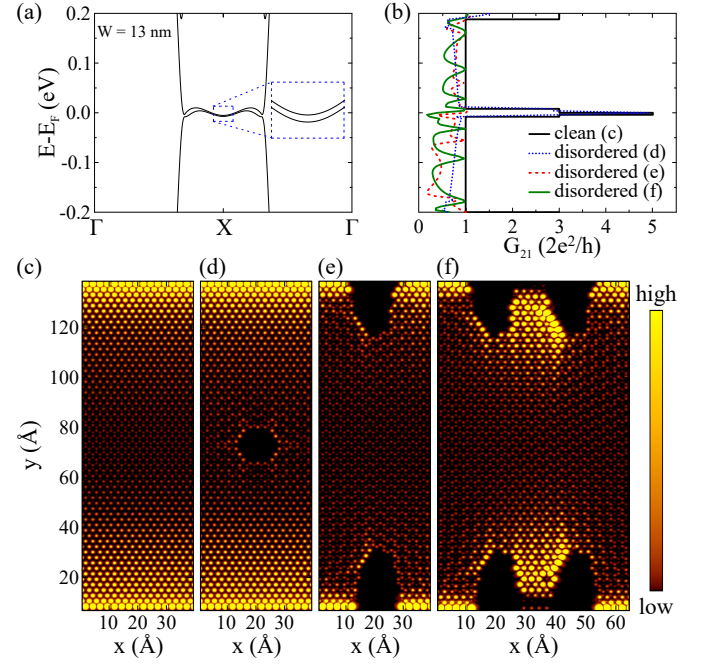


FIG. 3. (Color online) (a) *Ab initio* band structure; (b) the corresponding zero-temperature two-terminal conductance G_{21} ; and (c)–(f) LDOS at $E - E_F = 0$ for an infinite G/hBN wire with zigzag edges. The wire is clean in (c), it includes bulk nanopore in (d), or edge disorder in (e) and (f). The wire of width $W = 13$ nm is described by a DFT Hamiltonian, as implemented in the ATK [50] package, in the basis of double-zeta polarized pseudoatomic orbitals on C, B, N and edge passivating H atoms, and local density approximation is used for the exchange-correlation functional. For comparison, the same panels for an isolated graphene wire with zigzag edges are provided in Fig. S3 in the SM [30].

equilibrium [3], but they would become mediative VH currents connecting the two crossbars in Fig. 1 under the application of bias voltage, thereby circumventing the absence of electronic states around the DP while demanding *a major overhaul of the LB theory* [20] in which the absence of states within the gap is a fundamental reason for $R_{NL} \equiv 0$ in Fig. 2(c). In geometries with $L < W$, we do get $R_{NL} \neq 0$ in Fig. 2(c) (see also Ref. [18]), but this is trivially explained by transport through evanescent wave-functions propagating from first to second crossbar through the gap in such geometries [12, 18].

Another *long-standing puzzle* is the metallic-like ordinary longitudinal resistivity, $\rho_{xx} \sim 10$ k Ω , measured experimentally [1] for the G/hBN channel between the two crossbars despite the expected finite gap in its bulk. This suggests the presence of additional conduction pathways, such as edge currents observed very recently [24], which shunt the highly insulating state at low temperatures. However, previous theoretical studies have concluded that edge states are either absent [3] or, when they are present due to edges like zigzag [25, 26] or chiral [27, 28], they become gapped near the DP and

dispersionless away from it so they are unable to carry any current [29]. The latter conclusion is reproduced in Fig. S1(f) in the Supplemental Material (SM) [30] where we compute band structure of G/hBN wire with zigzag edges using the same simplistic Hamiltonian employed in prior theoretical studies [1–4, 15, 18, 29].

In this Letter, we resolve *both* puzzles— $R_{\text{NL}} \equiv 0$ [Fig. 2(c)] obtained for multiterminal G/hBN whose bulk counterpart exhibits $\sigma_{xy}^v \neq 0$; and metallic-like ρ_{xx} despite presumed gap opening around the DP—by performing density functional theory (DFT) calculation combined with quantum transport simulations, based on both the multiterminal LB formula (Figs. 2 and 3) and the Kubo formula (Fig. 4). We demonstrate that these puzzles are an artifact of the simplistic Hamiltonian [1–4, 15, 18, 29], which provides inadequate description of G/hBN wires. For example, in contrast to previously obtained [29] gapped band structure for all types of G/hBN wires, the *ab initio* band structure [Fig. 3(a)] of G/hBN wires with zigzag edges has no gap. Furthermore, the *ab initio* Hamiltonian combined with the LB formula yields R_{NL} [Fig. 2(a)] and ρ_{xx} in [Fig. 2(d)] whose features are *remarkably similar* to their counterparts measured in Ref. [1], such as ρ_{xx} peak being wider than R_{NL} peak whose centroid is slightly shifted to the left of the DP.

Since the resolution of the two puzzles relies on an accurate Hamiltonian for G/hBN wires, as well as its combination with a proper quantum theory for observable transport quantities, we first summarize inconsistencies arising in previous theoretical analyses. A putative “standard model” [1–4, 15] of G/hBN is gapped Dirac Hamiltonian describing single valley, $\hat{H}_{\text{D}} = \hbar v_F(\hat{\boldsymbol{\sigma}} \cdot \hat{\mathbf{k}}) + \Delta \hat{\sigma}_z$, where v_F is the Fermi velocity, $\hat{\boldsymbol{\sigma}} = (\hat{\sigma}_x, \hat{\sigma}_y)$ is the vector of the Pauli matrices corresponding to the sublattice degree of freedom and $\hbar \hat{\mathbf{k}}$ is the momentum operator. The seminal arguments [2] for the VHE in gapped Dirac systems are based on semiclassical transport theory describing the motion of a narrow wave-packet constructed by superposing [2, 43] eigenstates of \hat{H}_{D} with dispersion $\epsilon_{\mathbf{k}}$. The wave-packet velocity [13], $\mathbf{v}_{\mathbf{k}} = \frac{1}{\hbar} \partial \epsilon_{\mathbf{k}} / \partial \mathbf{k} + d\mathbf{k}/dt \times \boldsymbol{\Omega}_{\mathbf{k}}$, acquires an anomalous term due to the Berry curvature $\boldsymbol{\Omega}_{\mathbf{k}}$ hot spot near the apex of the valley described by \hat{H}_{D} . Since $\boldsymbol{\Omega}_{\mathbf{k}}$ in valley K has opposite direction to that in valley K' , electrons belonging to two valleys will be separated [43] in the opposite transverse directions in the presence of an applied electric field \mathbf{E} which is required to accelerate electrons according to $\hbar d\mathbf{k}/dt = e\mathbf{E}$. This gives rise [2] to $\sigma_{xy}^{K,K'} = \frac{e^2}{\pi \hbar} \int d^2k f(\epsilon_{\mathbf{k}}) \Omega_{\mathbf{k}}$, where $f(\epsilon_{\mathbf{k}})$ is the Fermi function forcing the integration over the whole Fermi sea, i.e., from the bottom of the band to the Fermi level E_F . f

However, it has already been pointed out in Ref. [18] that nonzero \mathbf{E} *cannot* appear in the linear-response limit of the multiterminal LB formula [19–21]. The experiments measuring R_{NL} are carefully kept [1] in the

linear-response regime in order to avoid heating of the device and the ensuing thermoelectric effects that can add large spurious contributions to R_{NL} [7]. The multiterminal LB formula, $I_p = (2e^2/h) \sum_q G_{pq}(V_p - V_q)$, relates the total charge current I_p in lead p to voltages V_q in all other leads *via* the conductance coefficients $G_{pq} = \int dE (-\partial f / \partial E) T_{pq}(E)$, where the derivative of the Fermi function confines the integration to a shell of states of width $\sim k_B T$ around E_F [20]. The transmission functions $T_{pq}(E)$ do not include any effect of \mathbf{E} [19–21]. We use the multiterminal LB formula implemented in KWANT package [21, 44] to compute V_{NL} and R_{NL} in response to an injected current $I_3 = -I_4$ [12] while keeping $I_p \equiv 0$ in the other four leads. The same procedure allows us to compute $\rho_{xx} = R_{4\text{T}} W / L$ from the four-terminal resistance $R_{4\text{T}} = (V_3 - V_4) / I_1$ obtained by injecting current $I_1 = -I_2$ into the device in Fig. 1 and by imposing voltage probe condition, $I_p \equiv 0$, in leads $p = 3-6$.

The semiclassical arguments for the origin of σ_{xy}^v can be replaced by quantum transport theory based on the Kubo formula [15, 45], which requires to first obtain [46, 47] the velocity operator $\hat{\mathbf{v}}$ for the chosen Hamiltonian. The physical consequences of the equation of motion for $\hat{\mathbf{v}} = v_F \hat{\boldsymbol{\sigma}}$ defined by \hat{H}_{D} [15]

$$\frac{d\hat{\mathbf{v}}}{dt} = \frac{1}{i\hbar} [\hat{\mathbf{v}}, \hat{H}_{\text{D}}] = 2v_F^2 (\hat{\mathbf{k}} \times \hat{\boldsymbol{\sigma}}) - \frac{E_g}{\hbar} \hat{\mathbf{v}} \times \mathbf{e}_z, \quad (2)$$

are extracted by finding the expectation value of Eq. (2) in a suitably prepared wave-packet [43, 48] injected with initial velocity into G/hBN where it can propagate even in the absence of any external electric field [48]. The first term in Eq. (2) causes *Zitterbewegung* motion of the center of wave-packet, while the second one acts on it like a Lorentz force due to an effective magnetic field in the direction of the unit vector \mathbf{e}_z perpendicular to the graphene plane. For electrons from the K' valley, $\hat{v}_y = -v_F \hat{\sigma}_y$, leading to opposite direction of such force.

The gapped Dirac Hamiltonian \hat{H}_{D} is a long wavelength limit of a more general tight-binding Hamiltonian (TBH) which accounts for both valleys and can, therefore, be used to capture intervalley scattering effects. This Hamiltonian, which is preferred for numerically exact calculations using the LB [18] or the Kubo formula (as well as for numerical simulations of wave-packet dynamics [43]), is defined on a honeycomb lattice with the lattice constant $a_0 \approx 2.46$ Å and a single p_z orbital per each carbon atom

$$\hat{H}_{\text{TB}} = \sum_i \epsilon_i \hat{c}_i^\dagger \hat{c}_i - \gamma_0 \sum_{\langle ij \rangle} \hat{c}_i^\dagger \hat{c}_j. \quad (3)$$

Here \hat{c}_i^\dagger (\hat{c}_i) creates (annihilates) an electron at site i ; hopping $\gamma_0 = 2.7$ eV is nonzero between nearest-neighbor (NN) carbon atoms; and the on-site energy $\epsilon_i = \pm \Delta$, responsible for the gap $E_g = 2\Delta$, is positive on one atom of the graphene unit cell and negative on the other one

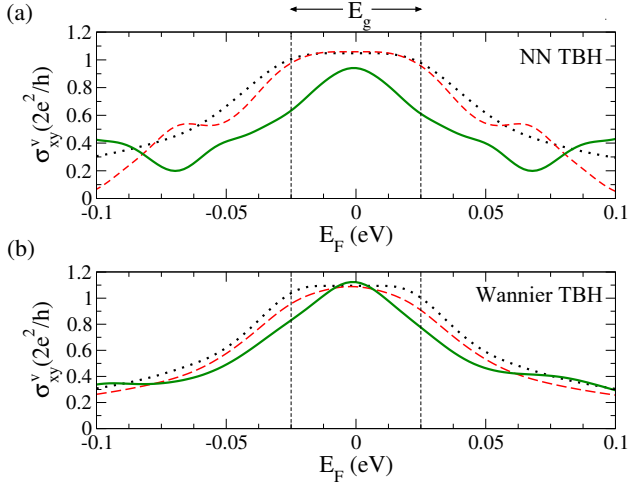


FIG. 4. (Color online). Zero-temperature VH conductivity σ_{xy}^v computed by the Kubo formula for a 2048×2048 G/hBN supercell described by: (a) NN TBH in Eq. 3; or (b) *ab initio* Wannier TBH. The dotted black line plots the clean case; red dashed line includes long-range disorder (with range $\xi = 10 \times a/\sqrt{3}$ and strength $U_p = 1.275$ eV in the model of Ref. [49]); and solid green line includes short-range disorder (with range $\xi = 0.1 \times a/\sqrt{3}$ and strength $U_p = 1.275$ eV in the model of Ref. [49]). The impurity concentration is 30% for both long- and short-range disorder.

to take into account the staggered potential induced by the hBN substrate (while neglecting any reorganization of chemical bonding or change in the atomic order of graphene and hBN layers). We use $\Delta = 29$ meV [14] to compute R_{NL} in Fig. 2(c) for G/hBN channel with zigzag edges, as well as to compute its band structure in Fig. S1(f) in the SM [30] exhibiting gapped flat bands around the DP [29].

Figure 4(a) shows σ_{xy}^v , computed using the Kubo formula [45, 47] combined with a valley-projection scheme [10, 30], for a square supercell of G/hBN with periodic boundary conditions described by \hat{H}_{TB} in Eq. (3). The supercell is either clean or it contains long- or short-range disorder, modeled following Ref. [49], as additional terms in the on-site energy ε_i . In the clean limit, we confirm [15] that $\sigma_{xy}^v = 2e^2/h$ is quantized inside the gap [Fig. 4(a)], as well as that the Fermi sea states just beneath the gap provide the main contribution to it [3]. For long-range disorder that does not mix valleys, σ_{xy}^v remains close to the clean limit within a smaller energy range than E_g [Fig. 4(a)] due to disorder-induced broadening of the states [15]. High concentration of valley mixing short-range disorder slightly reduces σ_{xy}^v [Fig. 4(a)].

In order to replace \hat{H}_{TB} with a more accurate Hamiltonian, we proceed by computing the *ab initio* band structure of G/hBN wires using local-orbital pseudopotential DFT, as implemented in ATK [50] and OpenMX [51, 52] packages, whose Kohn-Sham Hamiltonian can be also easily combined with the LB formula [53]. We assume

stacking where one C atom is over a B atom and the other C atom in the unit cell is centered above the hBN hexagon, as energetically most stable configuration found in DFT calculations [14]. The DFT Hamiltonian for a wire—composed of C, B and N atoms, as well as H atoms passivating dangling bonds along the zigzag edges—produces the gapless band structure in Fig. 3(a) and the corresponding zero-temperature two-terminal conductance $G_{21} = 5 \times 2e^2/h$ [Fig. 3(b)] near the DP (at $E - E_F = 0$). This value is insensitive to the bulk nanopore [Fig. 3(d)], signifying edge transport, but it is reduced to $G_{21} \lesssim 2e^2/h$ in the presence of edge vacancies [Fig. 3(e)] or quantum interferences generated by edge vacancies in series [Fig. 3(f)] due to lack of topological protection against backscattering [29, 55]. The valley-polarized states [54] above and below the DP are bulk states since G_{21} is reduced at those energies by the presence of the bulk nanopore [Fig. 3(d)]. The edge state are visualized by plotting the local density of states (LDOS) in Figs. 3(c)–(f), which is peaked near the edges but it remains nonzero in the bulk [28]. This can be contrasted with topologically protected edge states in quantum (ordinary [10], spin [56] and anomalous [57]) Hall insulators where LDOS in the bulk vanishes. The corresponding local current distributions (Fig. S4 in the SM [30]) shows that edge currents can survive edge disorder breaking G/hBN wire into short zigzag-edge segments, as suggested also by experiments [24].

Since the usage of the full DFT Hamiltonian is prohibitively expensive for large number of atoms ($\sim 10^6$ in our LB or Kubo formula calculations), we use DFT calculations to derive simpler *ab initio* TBHs [58]. A widely-used approach for this purpose (which retains faithfully the overlap matrix elements and their phases, orbital character of the bands and the accuracy of the original DFT calculations [58]) is to transform the DFT Hamiltonian to a basis of maximally localized Wannier functions in a selected energy window around E_F [59]. We combine Wannier TBH (truncated [58] to third NN hoppings without loss of accuracy of band structure in the interval considered in Fig. 4) with the Kubo formula in Fig. 4(b) where we find quantized σ_{xy}^v in the gap, as well as its surprising resilience to short-range disorder that was not exhibited in Fig. 4(a) for the simplistic TBH in Eq. (3). However, the Wannier TBH applied to G/hBN wires generates much larger group velocity $\partial\varepsilon_{k_x}/\hbar\partial k_x$ of edge state bands near the DP (Fig. S1(d) in the SM [30]) than the DFT Hamiltonian [Fig. 3(a)]. This is due to the fact that bulk DFT calculations (see the SM [30]) from which the Wannier TBH is derived do not include information about atoms (like H) passivating bonds of edge carbon atoms, which effectively changes the on-site energy in TBH along the edge [55]. Nevertheless, the Wannier TBH could be useful for fully encapsulated G/hBN wires where edges are not exposed to the environment [1, 24].

Therefore, we derive another *ab initio* TBH that pre-

cisely fits (Fig. S1(c) in the SM [30]) the bands around the DP in Fig. 3(a). This requires up to the fifth NN hoppings and on-site energies in Eq. (3), with adjusted values along the edges (Fig. S2 in the SM [30]). The *ab initio* 5NN TBH combined with the multiterminal LB formula yields R_{NL} exhibiting sharp peak [Fig. 2(a)] near the DP in the case of ballistic G/hBN channel. The introduction of edge disorder reduces the height of the peak [Fig. 2(a)], while concurrently generating peak of ρ_{xx} [Fig. 2(d)]. The maximum value of ρ_{xx} [Fig. 2(d)] is an order of magnitude larger than the measured one in Ref. [1], but it can be modulated using different types of disorder (our choice for edge disorder is illustrated in Fig. S4(b) in the SM [30]). Although metallic-like ρ_{xx} could arise due to trivial reasons, such as charge inhomogeneity induced by chemical or electrostatic doping, very recent imaging [24] of proximity-induced supercurrents flowing within narrow strips near the edges of G/hBN wires is in full agreement with LDOS [Fig. 3(c)–(f)] or local current distributions (Fig. S4 in the SM [30]).

In conclusion, R_{NL} peak exists in the ballistic limit [where $\rho_{xx} \rightarrow 0$ in Fig. 2(d)] and is reduced by short-range disorder [Fig. 2(a)], whereas σ_{xy}^v is insensitive to short-range disorder at the DP [Fig. 4(b)]. This suggests that these two quantities are not related to each other in a way conjectured by Eq. (1), thereby strengthening our principal conclusion—the observed R_{NL} is driven by particular gapless band structure and its edge eigenstates at the Fermi level tuned near the DP, rather than by the Fermi sea dissipationless topological valley currents [1, 3, 4] conjectured for the gapped Dirac spectra.

We thank I. V. Borzenets and K. Komatsu for insightful discussions. J. M. M.-T., X.-L. S. and B. K. N. were supported by NSF Grant No. CHE 1566074. J. M. M.-T. also acknowledges support from Colciencias (Departamento Administrativo de Ciencia, Tecnología e Innovación) of Colombia. J. H. G. and S. R. were supported by: the European Unions Horizon 2020 research and innovation programme (Grant No. 696656); the Spanish Ministry of Economy and Competitiveness and the European Regional Development Fund [Project No. FIS2015-67767-P (MINECO/FEDER)]; and by the Secretaria de Universidades e Investigación del Departamento de Economía y Conocimiento de la Generalidad de Cataluña, and the Severo Ochoa Program (MINECO, Grant No. SEV-2013-0295). The supercomputing time was provided by XSEDE, supported by NSF Grant No. ACI-1053575, and by the Barcelona Supercomputing Center (Mare Nostrum), under PRACE Project No. 2015133194.

* bnikolic@udel.edu

[1] R. V. Gorbachev *et al.*, Science **346**, 448 (2014).

- [2] D. Xiao, W. Yao, and Q. Niu, Phys. Rev. Lett. **99**, 236809 (2007).
- [3] Y. D. Lensky, J. C. W. Song, P. Samutpraphoot, and L. S. Levitov, Phys. Rev. Lett. **114**, 256601 (2015).
- [4] J. C. W. Song, P. Samutpraphoot, and L. S. Levitov, PNAS **112**, 10879 (2015).
- [5] M. Beconcini, F. Taddei, and M. Polini, Phys. Rev. B **94**, 121408 (2016).
- [6] D. A. Abanin *et al.*, Science **332**, 328 (2011).
- [7] J. Renard, M. Studer, and J. A. Folk, Phys. Rev. Lett. **112**, 116601 (2014).
- [8] P. Wei *et al.*, Nature Mater. **15**, 711 (2016).
- [9] C.-L. Chen, C.-R. Chang, and B. K. Nikolić, Phys. Rev. B **85**, 155414 (2012).
- [10] A. Cresti, B. K. Nikolić, J. H. García, and S. Roche, Riv. Nuovo Cimento **39**, 587 (2016).
- [11] J. Balakrishnan *et al.*, Nature Phys. **9**, 284 (2013); J. Balakrishnan *et al.*, Nature Commun. **5**, 4748 (2014).
- [12] D. Van Tuan *et al.*, Phys. Rev. Lett. **117**, 176602 (2016).
- [13] D. Xiao, M.-C. Chang, and Q. Niu, Rev. Mod. Phys. **82**, 1959 (2010); N. Nagaosa, J. Sinova, S. Onoda, A. H. MacDonald, and N. P. Ong, Rev. Mod. Phys. **82**, 1539 (2010).
- [14] G. Giovannetti *et al.*, Phys. Rev. B **76**, 073103 (2007).
- [15] T. Ando, J. Phys. Soc. Jpn. **84**, 114705 (2015).
- [16] D. A. Abanin, A. V. Shytov, L. S. Levitov, and B. I. Halperin, Phys. Rev. B **79**, 035304 (2009).
- [17] S. Adam, P. W. Brouwer, and S. Das Sarma, Phys. Rev. B **79**, 201404 (2009); J. W. Klos and I. V. Zozoulenko, Phys. Rev. B **82**, 081414 (2010).
- [18] G. Kirczenow, Phys. Rev. B **92**, 125425 (2015).
- [19] M. Büttiker, Phys. Rev. Lett. **57**, 1761 (1986).
- [20] H. U. Baranger and A. D. Stone, Phys. Rev. B **40**, 8169 (1989).
- [21] C. W. Groth, M. Wimmer, A. R. Akhmerov, and X. Waintal, New J. Phys. **16**, 063065 (2014).
- [22] P. L. McEuen *et al.*, Phys. Rev. Lett. **64**, 2062 (1990).
- [23] A. Roth *et al.*, Science **325**, 294 (2009).
- [24] M. J. Zhu *et al.*, Nat. Commun. **8**, 14552 (2017).
- [25] X. Jia *et al.*, Science **323**, 1701 (2009).
- [26] K. K. Saha, M. Drndić, and B. K. Nikolić, Nano Lett. **12**, 50 (2012); P.-H. Chang, H. Liu, and B. K. Nikolić, J. Comput. Electron. **13**, 847 (2014).
- [27] C. Tao *et al.*, Nature Phys. **7**, 616 (2011).
- [28] P.-H. Chang and B. K. Nikolić, Phys. Rev. B **86**, 041406(R) (2012).
- [29] W. Yao, S. A. Yang, and Q. Niu, Phys. Rev. Lett. **102**, 096801 (2009); Y. Ren, Z. Qiao, and Q. Niu, Rep. Prog. Phys. **79**, 066501 (2016).
- [30] See Supplemental Material (which includes Refs. [31–42]) at <http://> for additional details of our DFT and Kubo formula calculations; derivation of *ab initio* TBHs; and additional figures showing band structure, conductance and LDOS of isolated graphene wires with zigzag edges or local current distribution for clean and edge disordered G/hBN wires with zigzag edges.
- [31] T. Ozaki and H. Kino, Phys. Rev. B **69**, 195113 (2004).
- [32] M. Schlipf and F. Gygi, Comp. Phys. Commun. **196**, 36 (2015).
- [33] L. A. Agapito, M. Fornari, D. Ceresoli, A. Ferretti, S. Curtarolo, and M. Buongiorno Nardelli, Phys. Rev. B **93**, 125137 (2016).
- [34] T. B. Boykin, M. Luisier, G. Klimeck, X. Jiang, N. Kharche, Y. Zhou, and S. K. Nayak, J. Appl. Phys. **109**,

- 104304 (2011).
- [35] L. Brey and H. A. Fertig, Phys. Rev. B **73**, 235411 (2006); H. Deshpande and R. Winkler, arXiv:1603.04329.
 - [36] L. P. Zârbo and B. K. Nikolić, EPL **80**, 47001 (2007).
 - [37] G. Kresse and J. Hafner, Phys. Rev. B **47**, 558 (1993).
 - [38] G. Kresse and J. Furthmüller, Comput. Mater. Sci. **6**, 15 (1996).
 - [39] P. E. Blöchl, Phys. Rev. B **50**, 17953 (1994).
 - [40] G. Kresse and D. Joubert, Phys. Rev. B **59**, 1758 (1999).
 - [41] E. Prada and G. Metalidis, J. Comp. Electron. **12**, 63 (2013).
 - [42] A. Cresti, R. Farchioni, G. Grosso, and G. P. Parravicini, Phys. Rev. B **68**, 075306 (2003).
 - [43] C. M. Puetter, S. Konabe, Y. Tokura, Y. Hatsugai, and K. Shiraishi, arXiv:1211.0150.
 - [44] KWANT, <https://kwant-project.org/>.
 - [45] A. Bastin, C. Lewinner, O. Betbeder-Matibet, and P. Noziers, J. Phys. Chem. Solids **32**, 1811 (1971).
 - [46] A. Ferreira and E. R. Mucciolo, Phys. Rev. Lett. **115**, 106601 (2015).
 - [47] J. H. García, L. Covaci, and T. G. Rappoport, Phys. Rev. Lett. **114**, 116602 (2015); J. H. García and T. G. Rappoport, 2D Mater. **3**, 024007 (2016).
 - [48] B. K. Nikolić, L. P. Zârbo, and S. Welack, Phys. Rev. B **72**, 075335 (2005).
 - [49] F. Ortmann, A. Cresti, G. Montambaux, and S. Roche, EPL **94**, 47006 (2011).
 - [50] Atomistix ToolKit (ATK) 2016.4, <http://www.quantumwise.com>.
 - [51] OpenMX 3.8, <http://www.openmx-square.org/>.
 - [52] T. Ozaki, Phys. Rev. B **67**, 155108 (2003).
 - [53] M. Brandbyge, J.-L. Mozos, P. Ordejón, J. Taylor, and K. Stokbro, Phys. Rev. B **65**, 165401 (2002); D. A. Areshkin and B. K. Nikolić, Phys. Rev. B **81**, 155450 (2010).
 - [54] A. Rycerz, J. Tworzydło, and C. W. J. Beenakker, Nature Phys. **3**, 172 (2007).
 - [55] J. Li, I. Martin, M. Büttiker, and A. F. Morpurgo, Nature Phys. **7**, 38 (2011).
 - [56] P.-H. Chang, M. S. Bahramy, N. Nagaosa, and B. K. Nikolić, Nano Lett. **14**, 3779 (2014); A. Cresti, D. Van Tuan, D. Soriano, A. W. Cummings, and S. Roche, Phys. Rev. Lett. **113**, 246603 (2014).
 - [57] X.-L. Sheng and B. K. Nikolić, Phys. Rev. B **95**, 201402(R) (2017).
 - [58] S. Fang, R. K. Defo, S. N. Shirodkar, S. Lieu, G. A. Tritsarolis, and E. Kaxiras, Phys. Rev. B **92**, 205108 (2015).
 - [59] N. Marzari, A. A. Mostofi, J. R. Yates, I. Souza, and D. Vanderbilt, Rev. Mod. Phys. **84**, 1419 (2012); A. A. Mostofi, J. R. Yates, Y.-S. Lee, I. Souza, D. Vanderbilt, and N. Marzari, Comp. Phys. Commun. **178**, 685 (2008).